Developing tools for assessing bend-twist coupled foils

J. Banks*, L. Marimon Giovannetti, S.R. Turnock, S.W. Boyd
*J.Banks@soton.ac.uk

1 Introduction

There are many applications where the ability of a foil to passively adapt to the experienced fluid loading could be advantageous. This includes wind or tidal turbine blades, high performance hydrofoils for sailing yachts, or marine propellers. If these foils could naturally adjust their angle of attack as the flow speed varies their efficiency could be improved without the need for active control systems (Nicholls-Lee & Turnock, 2007). The use of composite materials provides the opportunity to tailor the bend twist coupling of a structure to achieve these goals (P. Veers & Bir, 1998).

To allow such foils to be designed and assessed numerical tools such as finite element analysis (FEA) and computational fluid dynamics (CFD) will need to be coupled together in fluid-structure interaction (FSI) simulations, but currently there is a lack of a full coupling between the two for passive adaptive composites. In isolation there are many methods for the validation of FEA and CFD. However, there is a lack of experimental validation data for FSI investigations.

This paper details a set of experimental tests conducted on a NACRA F20 curved dagger board in the University of Southampton's RJ Mitchell wind tunnel. Digital image correlation (DIC) was used to measure the full field deflection at the board tip and particle image velocimetry (PIV) was used to capture the position and strength of the tip vortex. Preliminary CFD simulations of the rigid experimental geometry are compared to this data.

2 Experimental Data

The experiments were conducted in the 3.5 m x 2.4 m RJ Mitchell wind tunnel at the University of Southampton. This closed circuit tunnel operates at wind speeds of 4 to 40 ms^{-1} with less than 0.2% turbulence. A six component Nutem load cell balance is mounted on a turntable in the tunnel roof. This allows forces and moments to be measured in the turntable axis system about the balance centre 1.27 m below the tunnel roof. Figure 1 shows the cross-section of the wind tunnel at the position of the dynamometer.

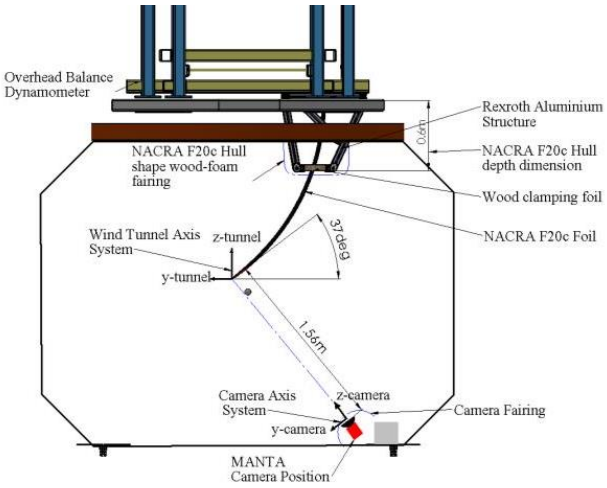

Figure 1 - Wind tunnel working section diagram.

2.1 Aerodynamic forces

The forces were measured at 1kHz and converted into the tunnel axis system to provide sideways lift coefficient (C_L), vertical force coefficient (C_Z) and drag coefficient (C_D).

An initial angle of attack sweep was completed to determine the zero lift condition of the board, and therefore the true zero degrees angle of attack (AoA) position allowing for board misalignment within the clamping structure. This determined the board was misaligned by 1.44 degrees from the turntable.

2.2 Board deflection

A stereo DIC system was set up in the wind tunnel allowing 3D deflection data to be captured within a 0.3x0.3m field of view at the board tip.

A background to this methodology and full details of this experimental setup can be found in (Giovannetti, Banks, Soubeyran, Turnock, & Boyd, 2014)

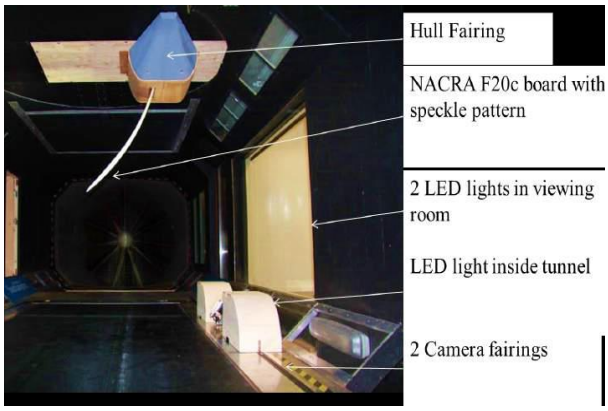

Figure 2 - DIC set up

2.3 Flow field measurement

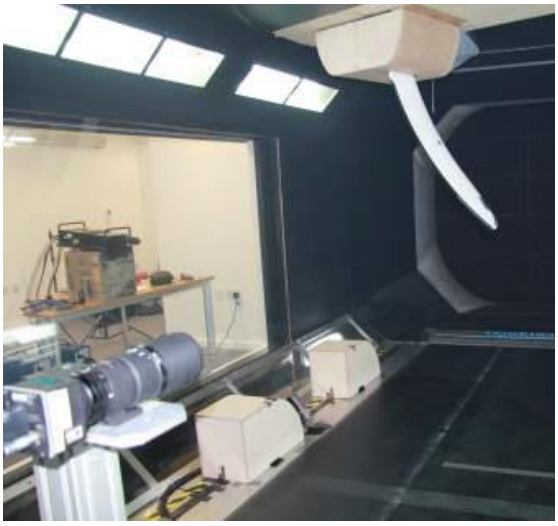

Figure 3 - PIV set up.

Particle image velocimetry allows two components of the fluid velocity to me measured on a plane using a single camera. Two images are taken of particles moving through a thin laser sheet, allowing the particle displacement, and therefore velocity, to be calculated (Raffel, Willert, Wereley, & Kompenhans, 2007).

A laser sheet was set up one chord (0.25m) behind the trailing edge of the foil and perpendicular to the flow direction. A 4 MP camera was positioned directly behind the board tip, with a 200mm Nikon lens providing a 0.2x0.2m field of view. Seeding particles were introduced into the tunnel using a smoke machine on a timer. The time between the two image frames was set to ensure that the majority of particles were observed in both frames. Then a series of 200 pairs of images were taken at a constant frame rate.

Two different angles of attack, 8.5 and 18.5 deg, were investigated at a range of wind speeds. The images were processed using the LaVision software DaVis.

3 Numerical simulations

Preliminary CFD investigations have focused on replicating the experimental results from the wind tunnel. Initially this has focused on simulating the un-deformed board geometry, along with the hull fairing. This will allow the impact of the blade deflection to be assessed by also simulating the deformed geometry at a later date.

3.1 Theoretical approach

A finite volume method is adopted for a single phase fluid. This method is derived from the surface integration of the conservative form of Navier Stokes' equations over a control volume. The incompressible Reynolds averaged Navier-Stokes (RANS) equations, written in tensor form, are defined as

$$\frac{\partial(\rho U_i)}{\partial t}+\frac{\partial(\rho U_i U_j)}{\partial x_j}=-\frac{\partial P}{\partial x_i}+\frac{\partial}{\partial x_j}\left[\mu\left(\frac{\partial U_i}{\partial x_j}+\frac{\partial U_j}{\partial x_j}\right)\right] - \frac{\partial}{\partial x_j}\left(\rho\overline{u'_i u'_j}\right)+f_i \qquad \textbf{3-1}$$

and

$$\frac{\partial U_i}{\partial x_i}=0 \qquad \textbf{3-2,}$$

for momentum and mass continuity respectively.

The effect of turbulence is represented in equation 3-1 by the Reynolds stress tensor $\rho\overline{u'_i u'_j}$ and is modelled using the k-omega SST turbulence model contained within OpenFOAM-2.2 (OpenFOAM®, 2011).

The SST model blends a variant of the k-ω model in the inner boundary layer and a

transformed version of the k-ε model in the outer boundary layer and the free stream (Menter, 1994).

3.2 Numerical model

A steady state solver was initially used with the solver settings and simulation parameters found in Table 3-1.

Table 3-1 - Numerical settings

Property	Mesh
Type of mesh	Unstructured (Hexahedral)
No. of elements	Approximately 7-8M
y+ on the foil	1-60
Domain Physics	kOmegaSST turbulence model, Automatic wall function
Boundary physics:	
Inlet	Free stream velocity of 30m/s
Outlet	Zero gradient
Bottom/side/top wall	Wall with free stream velocity
Board and fairing	Wall with no slip condition
Solver settings:	
Grad (U) Scheme	Gauss linear
Div (U)	Gauss limitedLinearV 1
Pressure coupling	SIMPLE
Convergence criteria	P 1e-7, U 1e-6, k 1e-8, omega 1e-8
Processing Parameters:	
Computing System	Iridis 4 Linux Cluster (University of Southampton)
Run type	Parallel (32 Partitions run on 2x16 core nodes each with 23 Gb RAM)

3.3 Meshing Technique

The simulation domain replicates the dimensions of the RJ Mitchel wind tunnel with 8 m upstream of the foil and 12 m downstream. The hull fairing is included to replicate the same flow over the board as in the experiment.

An unstructured hexahedral mesh around the foil was created using the snappyHexMesh utility within OpenFOAM. Firstly a coarse block mesh of hexahedral cells is created, using the blockMesh utility, defining the size of the domain and the initial cell size in each direction. Specific areas within the domain are then specified for mesh refinement in progressive layers. For each layer of refinement conducted each cell within the specified region is split into 8 equal parts, doubling the mesh density in all directions. Regions of refinement were placed around the foil, fairing and an estimated wake path. Two boundary layer elements are also grown out from the foil surface mesh. This localised refinement process results in a general mesh structure and boundary layer refinement that can be seen in Figure 4.

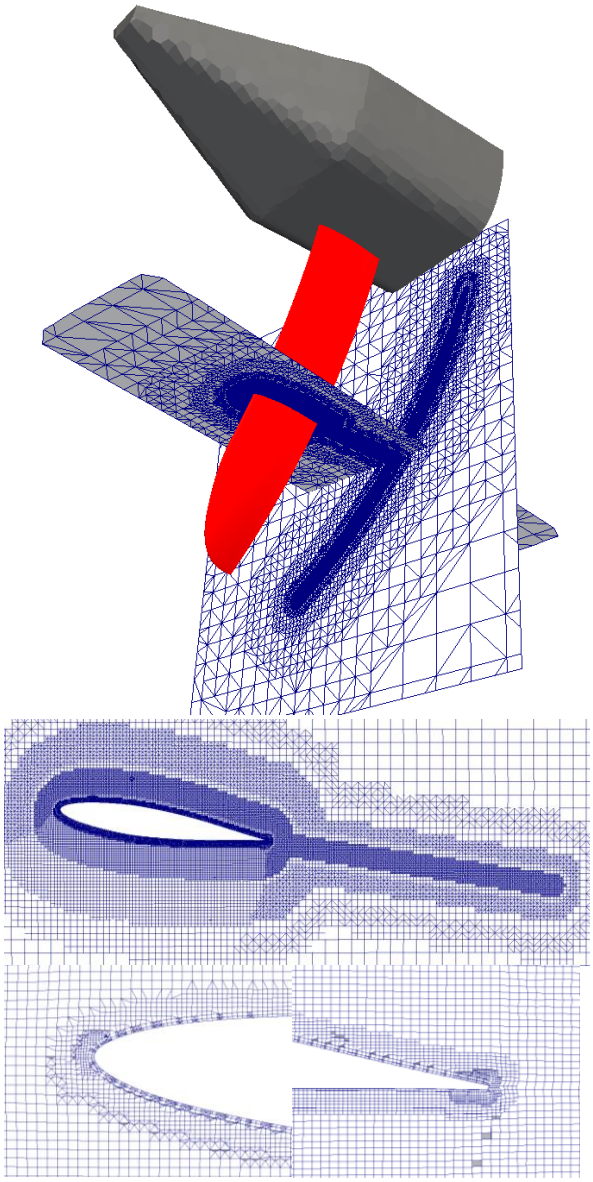

Figure 4 - Mesh structure

4 Results

An over view of the experimental results obtained in the wind tunnel is presented here and compared with preliminary CFD results.

4.1 Force comparison

The force coefficients from the CFD simulations are compared with experimental results in Figure 6. In general there is good agreement for the lift and drag coefficients for angles of attack less than 10 degrees. However a general trend of slightly over predicting the lift and under predicting the drag can be observed. In this region the flow is mainly attached with separation just starting to occur at an angle of attack of 8.5 degrees. This can be observed in the surface streamlines and y^+ distribution presented in Figure 5. The aligned flow and high y^+ over the majority of the suction side of the foil indicates that the flow is mainly attached for the first two thirds of the chord but with some separation towards the trailing edge. Some larger unsteady regions of separation can be observed towards the root of the board, potentially caused by the flow over the hull fairing.

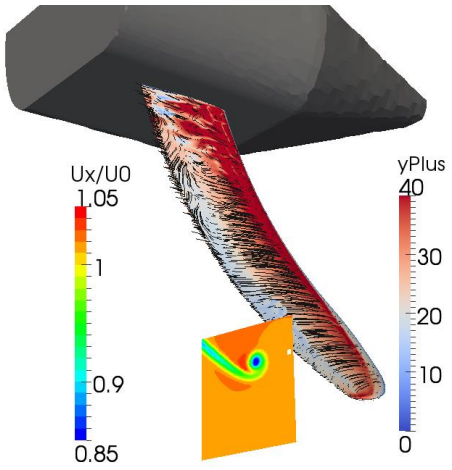

Figure 5 - y+ values on the board surface with AoA = 8.5 deg, with normalised axial velocity displayed on the PIV plane.

For large angles of attack, where the flow if fully separated, a large discrepancy is seen between the CFD and experimental data. It should be noted that the unsteady flow regime created by large amounts of separation requires an unsteady flow solver to accurately capture the flow physics.

A significant difference is also observed in the vertical force coefficient, Cz. As an assessment of board pitch angles was not completed in the wind tunnel it is possible that there was an error in the vertical alignment of the board in its clamps. The potential impact of this error should be investigated further using CFD simulations.

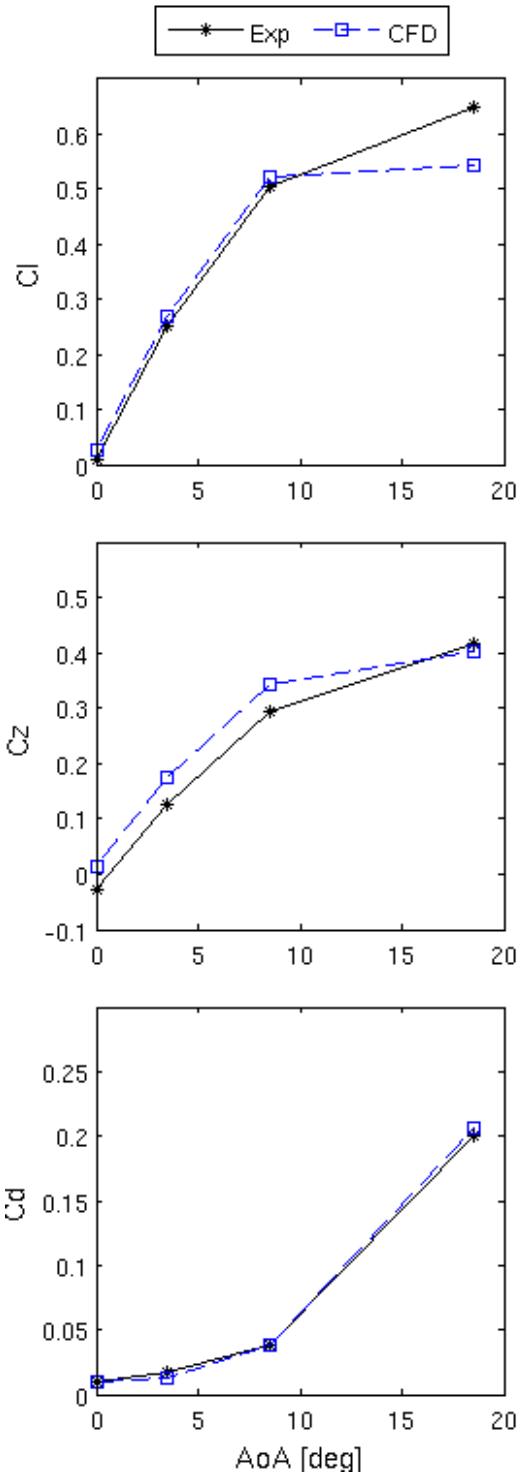

Figure 6 – Comparison of CFD force prediction against experimental data.

4.2 Deflection data

An example of the board tip deflection data obtained from the DIC system in the wind tunnel is provided in Figure 7. It is intended that both

this and twist data gathered and presented in (Giovannetti et al., 2014) can be used to generate deflected foil geometries allowing the impact of board bend and twist on performance to be assessed.

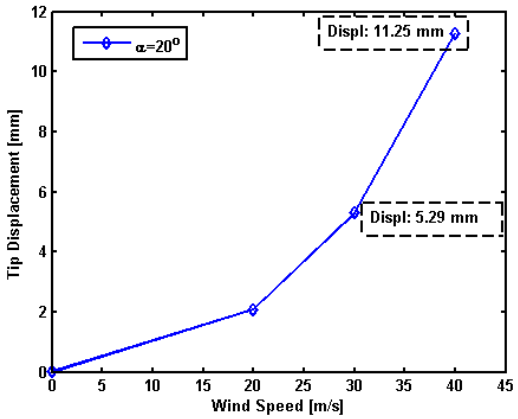

Figure 7 - Board tip deflection for an AoA of 18.5 deg.

4.3 Flow field comparison

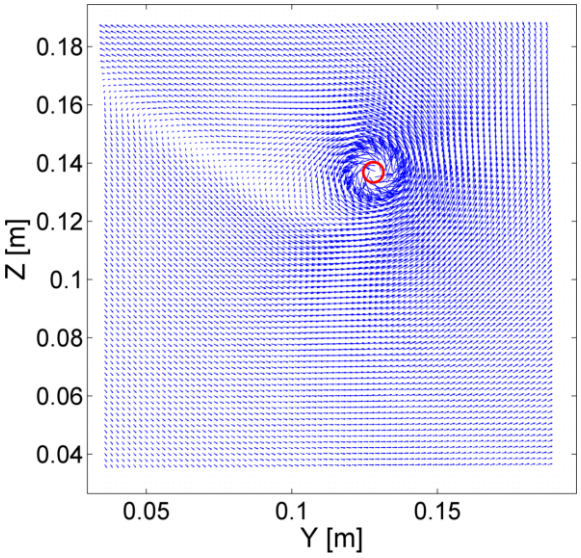

Figure 8 - Mean experimental velocity vector field, for AoA = 8.5 deg, with highlighted vortex centre.

An example of the mean transverse velocity vector field measured using the PIV system is provided in Figure 8. The basic VORTFIND algorithm, originally presented in (Pemberton R, Turnock S, Dodd T, 2002), was used to locate the centre of the tip vortex in the 200 vector fields produced for each experimental configuration The algorithm ranks which vectors are closest to the vortex centre using criteria defined in (Phillips & Turnock, 2013). The average position of the 10 closest vectors was then taken as the vortex position for each vector field. The average vortex position was then calculated and is highlighted in Figure 8.

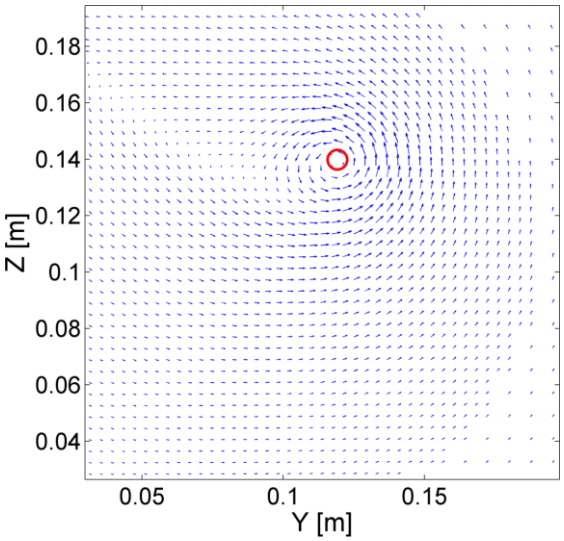

Figure 9 - CFD vector field for AoA = 8.5 deg, each vector represents 1 cell.

To compare the CFD results with the experimental flow field data the velocity components were sampled on the same plane as the laser sheet, see Figure 10. It appears that there is a slight discrepancy in the position of the vortex, possibly due to the experimental board deflection, however a much greater difference is observed in the local vortex velocities. This can be assessed by calculating the mean tangential velocity magnitude for different radiuses away from the vortex centre, see Figure 11.

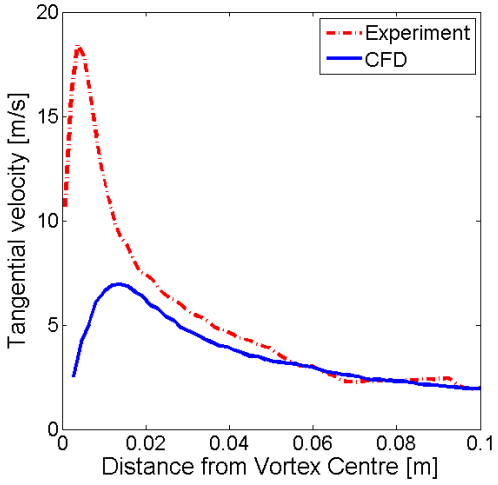

Figure 10 – Mean Tangential velocity for an AoA = 8.5 deg

It is clear that the vortex structure near the core is not well captured in the CFD. This is most likely due to lack of mesh density in this region, which can be observed in the vector spacing in Figure 9.

Both the mean and distribution of the experimental tip vortex position can be seen for different wind speeds and angles of attack in Figure 11. The impact of flow separation on the variability of the vortex position can be seen as the AoA increases. The impact of the board deflection can also be seen on the tip vortex position, especially for AoA = 18.5 deg.

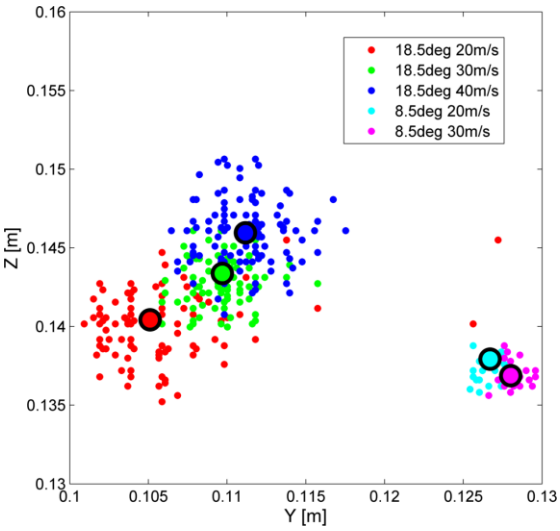

Figure 11 - Distribution of experimental tip vortex position for different wind speeds and angles of attack, with mean position highlighted by black ring.

5 Conclusions

A detailed set of experiments has been conducted providing validation data for both the structural response and fluid dynamic flow for a new fluids structure interaction test case. Preliminary CFD results are compared against these and significant future areas of improvement are identified.

6 Acknowledgements

The authors would like to thank the help of the TSRL team, Dave Hollis from LaVision, the RJ Mitchell wind tunnel staff and the research funding from the EPSRC (grant number EP/009876/1).

7 References

Giovannetti, L. M., Banks, J., Soubeyran, X., Turnock, S. R., & Boyd, S. W. (2014). Full-field deformation response of a high performance foil under fluid loading using Digital Image Correlation. *Ready for submission.*

Menter, F. R. (1994). Two-equation eddy-viscosity turbulence models for engineering applications. *AIAA-Journal*, *32*(8), 269–289.

Nicholls-Lee, R. F., & Turnock, S. R. (2007). Enhancing Performance of a Horizontal Axis Tidal Turbine using Adaptive Blades. In *OCEANS 2007 - Europe* (pp. 1–6). Aberdeen: Ieee. doi:10.1109/OCEANSE.2007.4302437

OpenFOAM®. (2011). *OpenFOAM – The Open Source CFD Toolbox- User Gide*, *Version 2.01*. Retrieved from www.openfoam.org

P. Veers, & Bir, G. (1998). Aeroelastic tailoring in wind-turbine blade applications. In *Windpower'98, American Wind Energy Association Meeting and Exhibition*. Bakersfield, California. Retrieved from http://windpower.sandia.gov/other/AWEA4-98.pdf

Pemberton R, Turnock S, Dodd T, R. E. (2002). A novel method for identifying vortical structures. *Journal of Fluids and Structures*, *16*(23), 1051–1057.

Phillips, A., & Turnock, S. (2013). Application of the VORTFIND algorithm for the identification of vortical flow features around complex three-dimensional geometries. *International Journal for Numerical Methods in Fluids*, *71*(11), 1461–1474. doi:10.1002/fld.3720

Raffel, M., Willert, C., Wereley, S., & Kompenhans, J. (2007). *Particle Image Velocimetry*.